EARTH SURFACE PROCESSES AND LANDFORMS
Earth Surf. Process. Landforms (2013)

Published online in Wiley Online Library
(wileyonlinelibrary.com) DOI: 10.1002/esp.3396

Recent effects of tidal and hydro-meteorological changes on coastal plains near the mouth of the Amazon River

José Tasso Felix Guimarães,[1,2]* Marcelo Cancela Lisboa Cohen,[2] Marlon Carlos França,[2] Luiz Carlos Ruiz Pessenda,[3] Eduardo deJesus Souza,[2] Afonso César Rodrigues Nogueira[2] and Ronnie Alves[1]
[1] Instituto Tecnológico Vale, Belém, PA Brazil
[2] Programa de Pós-Graduação em Geologia e Geoquímica, Universidade Federal do Pará, Belém, PA Brazil
[3] Centro de Energia Nuclear na Agricultura (CENA), Piracicaba/SP, Brazil

Received 2 February 2012; Revised 21 December 2012; Accepted 24 January 2013

*Correspondence to: José Tasso Felix Guimarães, Instituto Tecnológico Vale. Travessa Boaventura da Silva, n 955, 3 andar (Umarizal), 66055-090 Belém, Pará, Brazil. E-mail: tasso.guimaraes@vale.com; tasso@ufpa.br

ESPL
Earth Surface Processes and Landforms

ABSTRACT: The goal of this work was to understand the main hydrodynamic processes acting on tidal flats of the coast of Amapá near the mouth of the Amazon River, and how they change over the short term (~ 20 years). The analysis of morphological and geobotanical units was carried out by applying processing and interpretation methods to optical and synthetic aperture radar (SAR) images, combined with data on water salinity, maximum flood height, sedimentary facies data, rainfall and river discharge. The temporal analysis of morphological and geobotanical units suggests the relative stabilization of savannah, 'várzea' and mangrove areas during the drier period and increasing tidal amplitude between 1987 to 1997. The wetter period and decreasing tidal amplitude between 1997 to 2008 led to an increase in the area of 'várzea' and lakes over savannah, and the expansion of mangroves mainly over the inundated field and tidal mud/mixed flats. Therefore, the decrease in rainfall index during the drier period is well-correlated with the reduction of the Calçoene River discharge and jointly with increasing tidal amplitude favored the increase of migration rate of the mud bank and erosion profile along the littoral. It was followed by the increase of the Calçoene River discharge and jointly with decreasing tidal amplitude during the wetter period, favoring the development of mangroves on muddy substrates near the coastline.

KEYWORDS: Amazon coast; remote sensing; sedimentology; mangrove; chenier ridges

Introduction

Sedimentary models commonly propose to the subdivision of modern tidal flats into supratidal, intertidal and subtidal environments in relation to different tidal water levels, each with a singular facies distribution (e.g. Klein, 1977; Reineck and Singh, 1980; Weimer *et al.*, 1982). These models have been successfully applied to tidal flats of the North Sea coast of Europe (e.g. Van Straaten, 1961; Reineck, 1975), Georgia coast (Basan and Frey, 1978), Gulf of California (Thompson, 1975), Bay of Fundy – Canada (Klein, 1970; Dalrymple *et al.*, 1978) and those associated with tide-dominated estuaries such as the Cobequid and Salmon – Canada (Dalrymple *et al.*, 1990; Lessa and Masselink, 1995), Ord, South Alligator, Mary and Louisa – Australia (Chappell and Woodroffe, 1994; Severn – UK (Allen, 1990), Gironde and Seine – France (Lesourd *et al.*, 2003). Morphostratigraphic studies of the northern Brazilian coast have resulted in the proposal of alternative models, in which modern tidal flats are the product of the filling process of coastal valleys (Cohen *et al.*, 2005; Souza Filho *et al.*, 2006), and supratidal environments correspond possibly to the topographically highest ancient zones (Souza Filho *et al.*, 2006).

The coastal plain of the Amapá is dominated by tidal flats that have a macrotidal regime (4–5 m amplitude) and are strongly influenced by the discharge from the Amazon River (Meade *et al.*, 1985; ANA, 2003; Gallo and Vinzon, 2005). The latter supplies about 20% of the particulate flow reaching the coast, in the form of shoreface-attached mud banks that tends to evolve to tidal mud flats, since mud banks act as a barrier to coastal erosion by significantly reducing the incident wave energy (Allison *et al.*, 1995; Jiang and Mehta, 1996). However, the deposition of muddy sediments has not been constant during the Holocene, allowing the development of several chenier ridges during intervening/inter-bank phases (e.g. Silveira, 1998; Baltzer *et al.*, 2004). Additionally, the Amapá tidal flats are part of the world's largest wetland system with mangrove vegetation, which extends for almost 2000 km between the São Marcos Bay (Brazilian coast) until the mouth of the Orinoco River (Kjerfve and Lacerda, 1993; Allison *et al.*, 2000; Fromard *et al.*, 2004). The continuity of the mangrove is interrupted in the zone influenced by Amazon River discharge, where the 'várzea' vegetation and herbaceous fields dominate (Guimarães *et al.*, 2010; Guimarães *et al.*, 2011).

Few studies have been conducted on these, the most extensive tidal flats of Brazil (e.g. Silveira, 1998; Santos, 2006), with research into fine-grained sedimentation generally restricted to the Amazon shelf and not the Amapá coastal plain (e.g. Nittrouer and Kuehl, 1995; Nittrouer *et al.*, 1995; Sommerfield *et al.*, 1995). Research into other parts of this muddy coast through French Guiana, Surinam and Guyana to the Orinoco, have attempted to analysis the interactions between mud and the hydrodynamic forcing, between mud and shoreline, and between mud and mangroves, in relation to the activity of waves, coastal currents and tides (e.g. 18·5 yr nodal cycle; Gratiot *et al.*, 2008), and the implications for sediment transport and balance, interactions with physico-chemical parameters and climatic event cycles (e.g. Allison and Lee, 2004; Baltzer *et al.*, 2004; Lefebvre *et al.*, 2004; Plaziat and Augustinus, 2004; Anthony and Dolique, 2006; Gratiot *et al.*, 2008; Anthony *et al.*, 2010).

In combination, these processes may have created one of the most extensive and most sedimentologically dynamic mangrove coasts in the world. Despite research in French Guiana and related to the Orinoco, that has expanded our knowledge of mud-bank shorelines (e.g. Anthony *et al.*, 2010 and references cited therein), the Amapá coast still remains poorly understood. Furthermore, the lack of accurate geomorphological data has created difficulties for subsurface interpretations. This study analyses morphological and geobotanical units along the Amapá coast, over the short term (~ 20 yr), based on processing and interpreting optical and synthetic aperture radar (SAR) images, and data on rainfall, river discharge, water salinity, maximum spring tide height and sedimentary facies; so as to understand the main climatic and hydrodynamic processes acting on tidal flats near the mouth of the Amazon River.

Study Area

Geological and physiographic setting

The study area is located in the Amapá Platform, which corresponds to emerged and submerged continental areas, continuously stable during several episodes of distension tectonics followed by the Gondwana break up and Equatorial Atlantic opening during the Jurassic/early Cretaceous (Szatmari *et al.*, 1987). The regional geology includes Mesoarchean-Devonian Crystalline and Metasedimentary rocks in the western region, and Pleistocene sandstone and conglomerates in the eastern region interpreted as tidal depositional systems (Souza, 2010). Erosional and depositional processes due to late Pleistocene and Holocene climatic and sea-level changes, jointly with tectonic processes, shaped the relief of the coast of Amapá, resulting in its current configuration (Lima *et al.*, 1991). Indeed, along the coastal plain adjacent to the Amazon River, extensive north-south trending Holocene terraces composed of sand and mud have developed (Figure 1a).

Geomorphological units are represented by Amapá hills and Pleistocene coastal plain in the hinterland, and Holocene fluviolacustrine and marine plains (unconsolidated sedimentary deposits) along the coast (Figure 1b). The floristic studies of Costa Neto and Silva (2004) and Carvalho *et al.* (2006) describe the geobotanical and land-use units. At the study site, a vegetation survey based on qualitative descriptions was carried out. Modern vegetation is thus characterized by savannah in the hinterland, 'várzea' (flooded freshwater forests) alluvial plains and small-scale tidal flats near the proximal portion of the Calçoene River, herbaceous fields in the supratidal flat and well-developed mangrove forests (intertidal flat) near the coastline (Guimarães *et al.*, 2013).

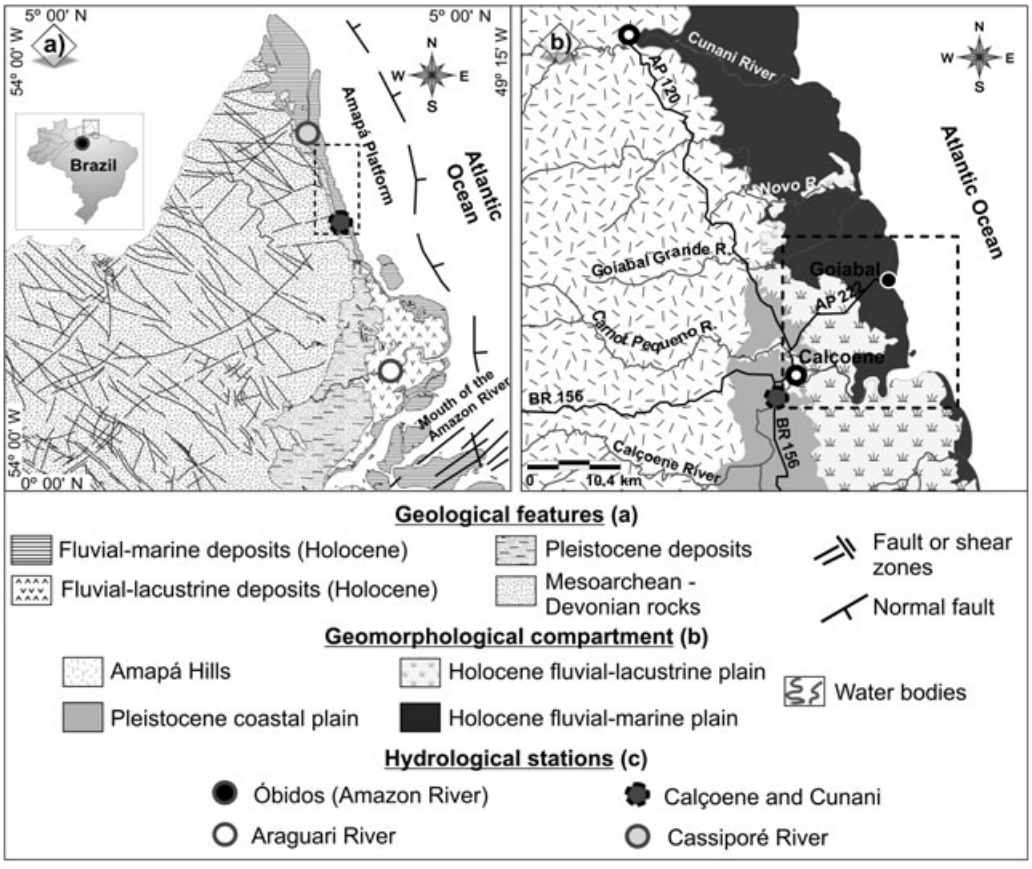

Figure 1. Study area: (a) regional geology [modified from CPRM (2010) and Costa *et al.* (2002)]; (b) regional geomorphology [modified from IBGE (2008)]

Climate and oceanographic setting

Regarding the variability of the climate system, the Intertropical Convergence Zone (ITCZ) gives rise to northeasterly and southeasterly trade winds. The ITCZ migrates meridionally during the year, reaching farthest north in August–September and coming closest to the Equator in March–April, exerting a significant control upon rainfall, wind and wave regimes (McGregor and Nieuwolt, 1998).

The regional climate is humid tropical characterized by dry (September to December) and rainy (January to July) seasons, with annual average precipitation and temperature around 3000 mm and 27 · 5 °C, respectively (Bezerra *et al.*, 1990). At the coast, wave directions are predominantly east and north-east, showing a very clear signal throughout the seasons, highly influenced by the trade winds, with their variation attributed to the seasonal migration of the ITCZ. Waves heights range from 1 to 2 m and periods of six to eight seconds. However, wave power in the Amazon coast has the lowest energetic levels of the Brazilian coast, with the most energetic conditions occurring during the wet season (Pianca *et al.*, 2010).

The mean discharge of the Amazon River is approximately 170,000 m^3/s (at the town of Óbidos), with maximum and minimum outflows of 270,000 and 60,000 m^3/s (ANA, 2003). This discharge contributes ~1 · 2 x 10^9 tons/yr of sediment (Meade *et al.*, 1985). However, new mean outflow estimation is approximately 203,000 m^3/s and sediment discharge about 754 x 10^6 tons/yr (Martinez *et al.*, 2009). The Amazon's estuary is classified as semidiurnal macrotidal (Pugh, 1987), with a tidal range of ~5 m (Gallo and Vinzon, 2005). The plume of the Amazon River is a seasonal feature extending ~3000 km into the Atlantic Ocean, and covers approximately 2 x 10^6 km^2 (Cooley *et al.*, 2007). The structure of the plume is controlled by the North Brazilian Current, which induces a north-western flow with speeds of 40–80 cm/s over the continental shelf (Lentz, 1995), strong tidal currents (Beardsley *et al.*, 1995), trade winds and the ITCZ (Lentz and Limeburner, 1995). Consequently, river discharge and hydrodynamic conditions allow a strong reduction of water salinity along the Amazon River and adjacent coast (Rosario *et al.*, 2009).

The mud supplied from the Amazon River is reworked seasonally and inter-annually on the Amazon shelf of Brazil (Amasseds, 1990) and is finally transported northwestward. Thus, 60–70% of this sediment is advected in a highly turbid suspension layer by tidal and local currents, and the rest migrates as shoreface-attached mud banks (Wells and Coleman, 1978; Lefebvre *et al.*, 2004). The Amapá coast appears to be the location of mud bank generation for the entire north-eastern coast of South America (Allison *et al.*, 2000). These mud banks are spaced at intervals of 15 to 25 km separated by inter-bank areas, are up to 5 m-thick, 10 to 60 km-long and 20 to 30 km-wide, and migrate along the Amazon-influenced muddy coast from 1 to > 5 km/yr (Gardel and Gratiot, 2005), in water depths of < 5 to 20 m over a modern upper shoreface mud wedge created from deposition of previous mud banks (Allison *et al.*, 2000).

Materials and Methods

Remote sensing data and image processing

The mapping, temporal and spatial analyses of morphological and geobotanical units were carried out by processing and interpretation methods in optical and SAR images, jointly with field surveys related to geomorphology and sedimentology. A set of six Landsat/TM images from 1987, 1997 and 2008 (225_58 and 225_68), one SAR/SRTM V2 image from 2000 and two SLAR/GEMS 1000 images from 1971 corresponding to the NA22VD and NA22XC sheets of the RADAM project (DNPM, 1971) were used for the remote sensing analysis (Table I).

The Landsat/TM images, obtained from the National Institute for Space Research – Brazil (INPE), were processed using the Spring 4.3 software (Câmara *et al.*, 1996) and geometrically corrected using another, previously corrected ETM + image. The mean squared error was 0 · 3 pixel and data re-sampling followed the nearest neighbor method. Radiometric correction was based on the minimum histogram pixel approach (Chavez, 1988). Regarding the squared error and using a simple rule of three, the geometric errors were obtained for each image and the cumulative error for each analyzed period. Thus, coastal changes less then 21 · 0 m (1987/1997) and 21 · 9 m (1997/2008) of linear distance and 0 · 0005 km^2 of area were not considered to spatial analysis of data (Table II). Image enhancements were applied based on linear and equalization stretches. Three bands for a red-green-blue (RGB) color composite (TM 4-5-6) were selected based on the optimum index factor scheme (Chavez *et al.*, 1982), and chosen for visual interpretation.

Table I. Main characteristics of the remotely sensed data

Platform	Sensor	Acquisition date	Angle of incidence	Spatial resolution (m)	Tidal condition
Twin-jet	GEMS 1000	1972	45°–77°	16	—
Landsat-5	TM	September 20, 1987	Nadir	30	Low (80 cm)
		September 15, 1997			Low (70 cm)
		August 28, 2008			Low (55 cm)
SRTM	InSAR	Fev. 2000	*Off*-nadir	90	—

Table II. Geometric and cumulative error of the images from 1987 to 2008

	Individual geometric error				Cumulative geometric error	
Acquisition date	Per area (km^2)	Linear (m)	RMS (per pixel)	Time interval	Per area (km^2)	Linear (m)
1987	0·0002	9·6	0·32	1987/1997	0·0005	21·0
1997	0·0003	11·4	0·38	1997/2008	0·0005	21·9
2008	0·0002	10·5	0·35			

These data were subsequently exported in shape file vector format for spatial analysis in the ArcMap 9.2 (ESRI, 2006) software. Validation was conducted with 50 ground control points obtained from a GPSMAP 60CSx GPS receiver, throughout the study site.

The SRTM data (C band, $\lambda = 5 \cdot 6$ cm) were acquired from the National Aeronautics and Space Administration (NASA), the National Imagery and Mapping Agency (NIMA), the German Space Agency (DLR) and the Italian Space Agency (ASI). Data were processed to improve their potential usefulness for geomorphological descriptions, including the customization of shading schemes and palettes using Global Mapper 8 (Global Mapper LLC, 2009). Development of such palettes was achieved through an interactive approach using display tools, which allowed highlighting of the morphological features of interest for this research according to on-screen observations (e.g. Hayakawa *et al.*, 2010). Morphometric analysis based on topographic profiles was applied to enhance the potential of feature visualization. These profiles are PathProfile/LOS command on Global Mapper 8 that selects the three-dimensional (3D) path profile/LOS (line of sight) tool as the current tool. This tool allows vertical profile along a user-specified path to be obtained from loaded elevation datasets.

SLAR/GEMS1000 data from NA22VD and NA22XC sheets (DNPM, 1971) were scanned at high resolution and stored in digital matrix format, which allowed data enhancements by the application of a gamma filter and the interpretation of ground features.

Sampling and facies description

Fieldwork was conducted during May 2009 (rainy season) and December 2010 (dry season) to validate the remote sensing data and to identify the main sedimentary processes acting at the study site. Hydrotopographic and water salinity measurements (e.g. Cohen, 2003), were carried out at 30 stations distributed along Goiabal road (AP 222) that intercept the main morphological and geobotanical units. These measurements use graduated rulers, where acrylic cylinders fixed at 10 cm intervals recorded the maximum height of spring tide in 2009 (DHN, 2009). The salinity of tidal water was measured with portable instruments *in situ*, without filtration. Local monthly rainfall data (Óbidos, Calçoene and Cunani station) and rivers discharges data (Amazon River – Óbidos station, Araguari and Cassiporé Rivers – Amapá stations) between January 1987 and December 2008, were acquired from HidroWeb (ANA, 2010). Statistical analyses were conducted using the R programming [1] language through the packages *stats*, *graphics* and *ellipses*. Distinct seasonal patterns were identified based on cluster (or time series) analysis of these data. The mean seasonal rainfall and river discharge (monthly average during the rainy and drier seasons), annual rainfall, total annual rainfall and river discharge (sum of seasonal means) were compared to recognize the influence of changes in hydro-meteorological parameters with morphological and geobotanical settings of the studied coast.

Sedimentary records comprise of surface features, exposed terraces, trenches and cores. Following the proposal of Walker (1992), facies analysis included descriptions of color, lithology, texture and structures. X-ray radiographs aided the identification of sedimentary structures. The interpretation of the sedimentological data in this work is also based on clastic tidalite process-response models (after Klein, 1971). The sedimentary facies was codified following Miall (1978).

Results

The geomorphologic analysis allowed the identification of two distinct compartments in the Calçoene coast presenting singular morphological and geobotanical setting: Pleistocene and Holocene compartments.

Coastal plain facies: geomorphic description, hydrodynamic and vegetation pattern

The Pleistocene compartment is bordered to the west by crystalline basement rocks related to the Amapá Hills, and to the east by the coastal plain. Considering that the wavelength of the C band interacts with canopy trees, resulting in elevations which reflect the combination of morphology and tree height (e.g. Hofton *et al.*, 2006), the Pleistocene compartment has an elevation of approximately 10 m (Figure 2) and presents a flat to very slightly undulated relief shaped by erosive processes with widely spaced hillocks, gullied as they approach low-order drainage channels, and terraces in zones proximal to the Calçoene River (Figures 3a and 3b). The shallow depressions receive deposition of colluvial clayey sand. This compartment is related to Pleistocene sedimentary rocks that overlap in lithological unconformity the Precambrian Crystaline Basement rocks marked by blocks and boulders and, often developing onlap contact (Souza, 2010).

Significant protuberance of an ancient shoreline in the form of a delta was identified at the study area. The feature covers an area of ~100 km^2 and likely preserves the main fluvial channel with SW-NE direction ('Goiabal Grande' River) that displays confined flow over the coastal plain. Additionally, another fluvial channel with NW-SE orientation was delineated, but fluvial flow is interrupted near the inundated fields of the Goiabal site (Figure 4). This feature, of birdfoot type, is likely comprised of six paleodeltaic lobes, and avulsion (complete and rapid abandonment of a fluvial channel, followed by the formation of a new channel) of the main fluvial channel from the deltaic system was also observed in this compartment. The avulsion process may also have been responsible for the partial or complete abandonment of several channels, which allowed the development of elongated lakes with SW-NE and SE-NW direction.

The paleochannels and low-order drainage channels are straight to meandering in pattern and they are sites to the development of 'várzea' and elongated lakes (Figures 2 and 3a). Paleochannels are common in this transitional sector, which consists of a thick peat layer (facies Pt), laminated mud, kaolinitic in nature (facies Ml), and cross-laminated sand (facies Sc) (Table III). The predominant vegetation units are 'várzea' with a total area of $190 \cdot 9$ km^2, and savannah with total area of $103 \cdot 2$ km^2. The 'várzea' also colonizes transitional sectors between the Pleistocene and Holocene plain (Guimarães *et al.*, 2013).

Tidal sedimentary facies predominate the Holocene compartment, that is approximately 10 km long and contains a tidal-fluvial channel, paleochannels, lakes, 'várzea', herbaceous fields, mangroves, elongated tidal mud bars (ETMB), chenier ridges, tidal mud and mixed (non-vegetated) flats (Figures 2 and 4). The main plant species are described in Guimarães *et al.* (2013).

Tidal-fluvial channel

This channel is represented by the Calçoene River that shows a 'straight' to meandering pattern, and water flow on basement crystalline rocks ('lajedos') in its proximal portion, contrasting with high sinuosity and a funnel shape in the distal portion (Figures 4 and 5a).

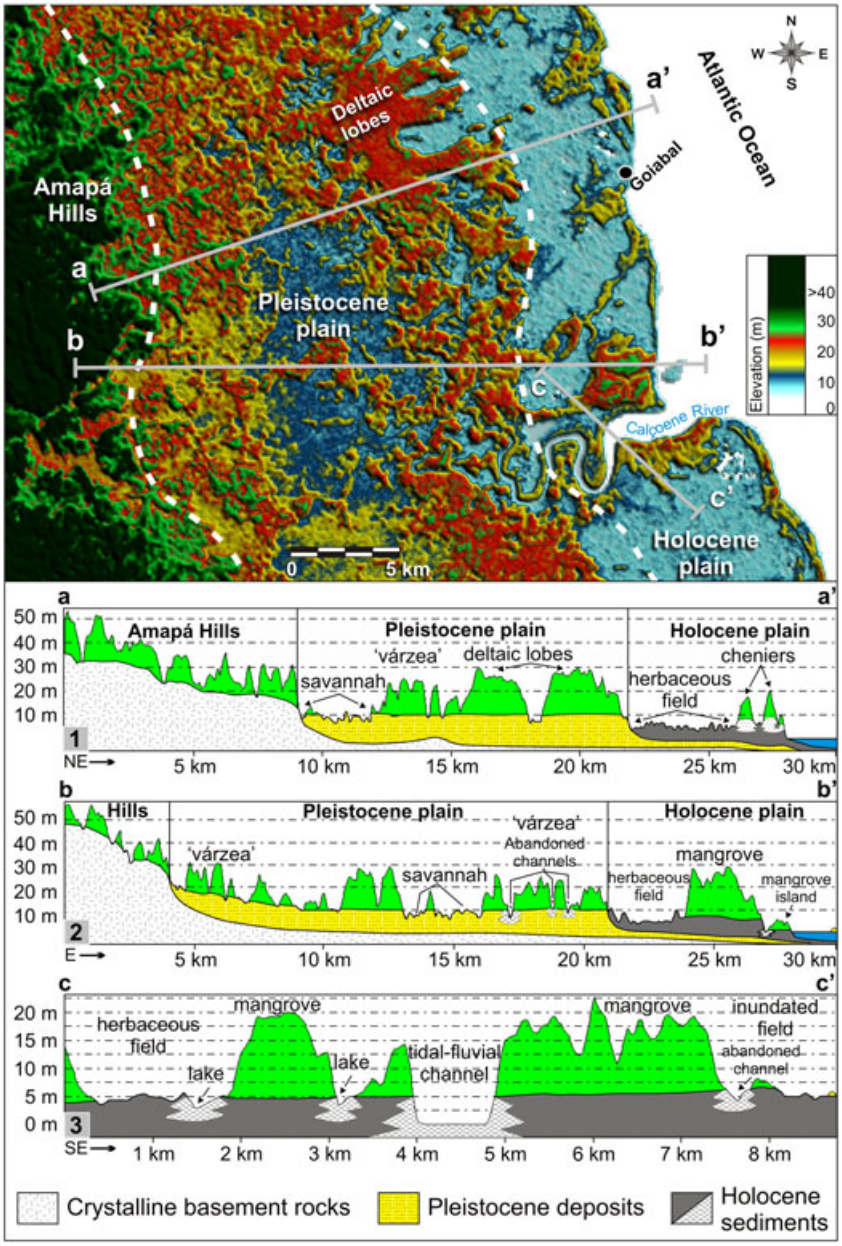

Figure 2. Digital elevation model of the Amapá Coast based on SRTM data with morphometric profiles along the morphological and geobotanical units. This figure is available in colour online at wileyonlinelibrary.com/journal/espl

The reversal in the flow of the Calçoene River by tidal flood currents may be effective up to ~20 km upstream from the mouth, during the drier season, which increases the temporary deposition (seasonally controlled) of muddy sediments and water turbidity in the proximal portion of the river. Water salinity is low, with maximum values of 5‰ near the mouth. There are only a few secondary channels along this river that remain active, and they represent a short extension. Large and small-scale point-bars and cut banks are frequent in the convex and concave margins of the river channel, respectively (Figure 5a). The point-bar deposit display inclined heterolithic lamination (facies Hi) with local residual granules, inclined (facies Mi) and bioturbated mud (facies Mb) (Figure 5b; Table III).

Abandoned channels and lakes

An extensive network of abandoned channels was identified in the coastal plain. The abandoned channels maintain the shape and typical concavity of the original channel, resulting in the formation of lakes and lake belts (Figures 5a, 5c and 5d). The lakes show SW-NE orientation, elevation between 1 and 3 m, around 1 m depth, water salinity of ~0‰ and ephemeral behavior due to the seasonality of climate and hydrology. The deposits consist of thick peat layers (facies Pt), laminated mud (facies Ml) and bioturbated mud (facies Mb; Table III).

'Várzea'

'Várzea' is located on narrow and seasonal tidal flats developed over granitic 'lajedos' in the proximal portion of the tide-dominated river, and it has an elevation of approximately 4 m and maximum water salinity ~2‰. Additionally, several elements of this unit may be recognized surrounding paleochannels and lakes of the coastal plain (Figures 5a and 5c; Guimarães *et al.*, 2013). The deposits present lenticular bedding (facies Hl) and bioturbated mud (facies Mb).

Herbaceous field

The herbaceous field covers an area of $67 \cdot 4\,km^2$, mainly colonized by herbaceous vegetation adapted to hydric stress (Guimarães *et al.*, 2013), since it is only flooded by a water column of 10 cm during overbank flow at higher spring tides of the rainy season (supratidal). This unit is also characterized by an elevation between approximately 2 and 4 m and low

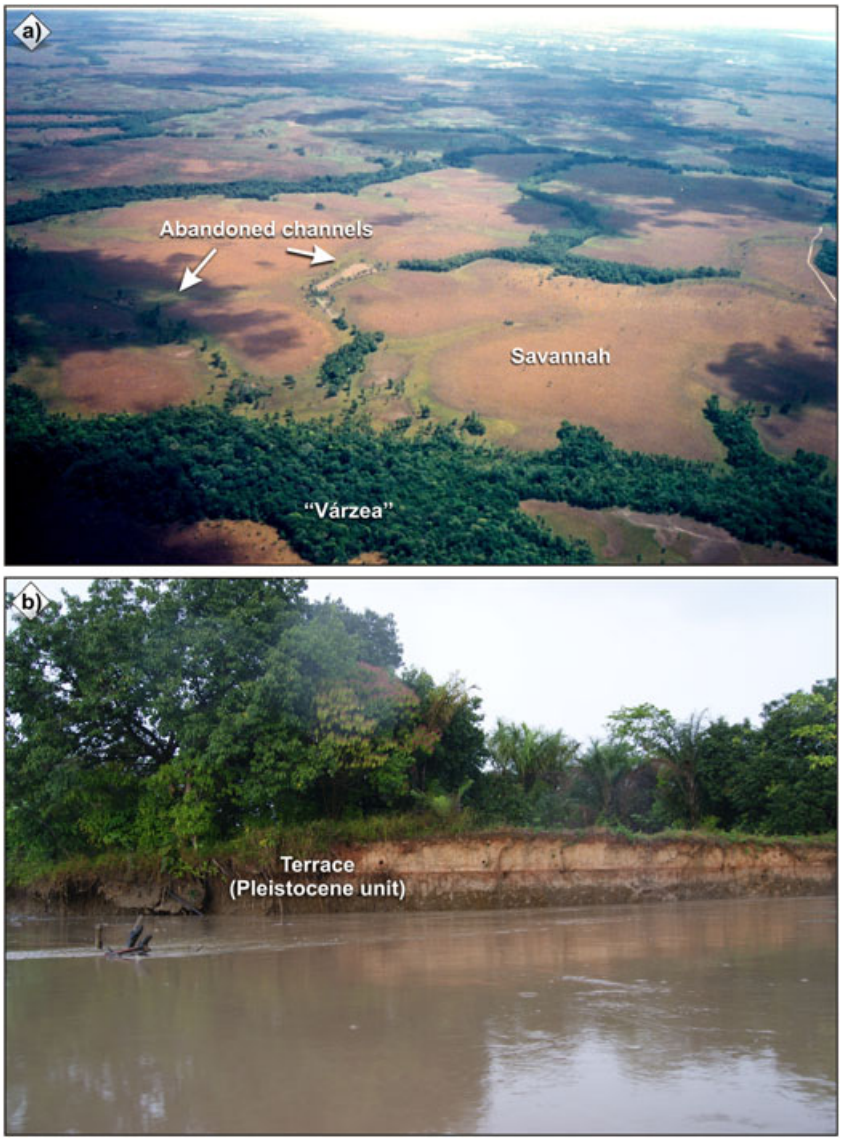

Figure 3. (a) Aerial view, 1992, of the lateral relationship between savannah, 'várzea' and paleochannels (courtesy of Professor Maria Thereza Prost) and (b) terrace of the Pleistocene plain in the proximal portion of the Calçoene River. This figure is available in colour online at wileyonlinelibrary.com/journal/espl

drainage density due to the silting of the tidal channels, which produces several paleochannels (Figures 5d and 6a). The active tidal channels have maximum widths and depths of 4 and 2 m, respectively, and water salinity ~2‰. The deposits consist of bioturbated mud (facies Mb) with the predominance of herbaceous roots and root marks. Well-developed mud cracks are frequent during the dry season.

Mangroves

Mangroves cover an area of $36 \cdot 7\,km^2$ and are restricted to the coastline, colonizing intertidal flats of the distal portion of the tide-dominated river and wider tidal channels of the coastal plain (Figure 6b). However, this unit shows limited lateral continuity likely due to the silting and rapid narrowing of the channels, which limit tidal flat drainage. Mangroves have upper intertidal portion flooded by a water column of ~20 cm (water salinity between 2 and 4‰) during high spring tides in the rainy season. The sediment is composed of wavy (facies Hw) and lenticular bedding (facies Hl), and bioturbated mud (facies Mb) with abundant plant debris (Figures 6c and 6d; Table III).

Elongated tidal mud bars (ETMB)

ETMB were identified near the mouth of the Calçoene River, consisting of muddy bodies with E-W orientation and 600 to 800 m in length. The advanced stage of mud bar stabilization is recognized by mangrove development (Figures 4 and 5c). The sediments consist of lenticular bedding (facies Hl) and bioturbated mud (facies Mb) (Table III).

Chenier ridges

Chenier ridges cover an area of $10 \cdot 1\,km^2$ at the study site, and represent extensive, straight to slightly curved sand bodies overlaid on mangrove and inundated field deposits, indicating an interruption of mud flat progradation (e.g. Augustinus, 1989). This feature has N-S and NW-SE orientation, elevation of about 4 m, 2 to 4 km in length with interridge spacing between 20 and 200 m and inner chenier ridges ~2 km from the modern coastline (Figures 5 and 6e). Additionally, some ridges occur at an angle of 25º to 30º to the normal orientation of the coastline. The deposits show bioturbated sand (facies Sb, Figure 6f). The intense bioturbation and mottling features prevented the identification of primary sedimentary structures, possibly related to large-scale cross-bedding (e.g. Augustinus *et al.*, 1989).

Tidal mud flats

Tidal mud flats (non-vegetated) were only observed near the mouth of the Calçoene River, where the substrate was not yet stabilized by pioneer mangrove and/or 'várzea' vegetation

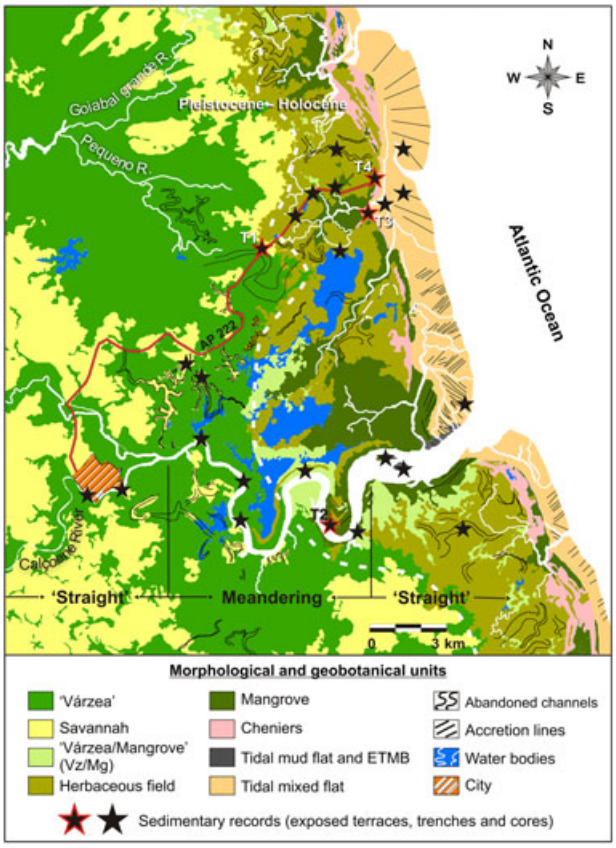

Figure 4. Geomorphological map of the Calçoene Coast with the location of sedimentary records consisting of exposed terraces, trenches and cores. Stars with a red outline correspond to the following lithological columns and figures described in the text: T3, Figure 6d; T4, Figure 6f. This figure is available in colour online at wileyonlinelibrary.com/journal/espl

(Figure 4). They comprise a small area of 0·7 km^2 and present numerous dewatering channels that can subsequently evolve into relatively deep subtidal channels bordered by arboreal strata. The sediments are represented by laminated mud (facies Ml) and lenticular bedding (facies Hl).

Tidal mixed flats

Tidal mixed flats (non-vegetated) encompass an area of 37·1 km^2, with NW-SE orientation and a relatively flat surface 0·5 to 2·5 km wide near the mouth of the Calçoene River (Figure 4). Longitudinal accretion lines were also observed. On this feature, plane beds with parting lineation produced by wave activity, ripples with multi-directional and continuous crests. In addition, were observed isolated ripples, several clay pebbles related to reworking of the flat during tidal channel dynamics that produces small-scale fallen blocks, daily modeled by tidal currents. Obstacle and moving tool marks, and beyond rill marks with a braided style are commonly identified. Tidal channels and mangroves undergoing siltation and burial processes, respectively, can also be recognized. Mixed flat deposits are represented by planar to quasi-planar fine to very fine sand (facies Sp), flaser, wavy and lenticular bedding (facies Hf, Hw and Hl, respectively; Table III).

Observed changes in hydro-meteorological parameters, morphological and geobotanical units (1987–1997 and 1997–2008)

The local monthly rainfall (LMF) and river discharge data (RDD) were aggregated to determine climate seasonal and temporal patterns. From a seasonal perspective, the data were split into rainy and dry seasons, while the pluri-annual ones (temporal perspective), into drier (1986–1997) and wetter (1998–2008) time intervals respectively. Discriminative patterns are observed in both box plots drawn from these patterns. Tall boxes indicate high variation while high boxes indicate high means. The true difference in means was statistically evaluated by a two sample *t*-test for each group of patterns to each local station. The corresponding *t*-values and *p*-values of the discriminative LMF and RDD patterns are presented in Table IV. Correlations were calculated using the Pearson product-moment correlation coefficient. In the correlation plots, positive correlation (blue colors) are depicted by ellipses bending to the right and negative correlation (red colors) by ellipses bending to the left. Additionally, a thinner ellipse means stronger correlation. The observed minimum and maximum correlations of the seasonal patterns range from –0·52 to 1 while the correlations of the temporal data range from –0·99 to 1.

The analysis of rainfall data of Calçoene and Cunani (Amapá coast), and Óbidos (Amazon River) stations from 1987 to 2008 clearly indicate two distinct climate seasons including a rainy season from December to May and dry season from June to November with some extreme events of drought and rainfall (Figure 7a). In the same way, river discharge data from Cassiporé and Araguari (Amapá coast), and Óbidos (Amazon River) stations also suggest some correlation with rainfall index between these two climate seasons (Figure 7b). It is reinforced by the correlation plot between all the hydro-metereological parameters used in this work (Figure 7c), which shows a very good seasonal correlation of rainfall and river discharge data from the Amapá coast and Amazon River station.

The temporal evaluation of changes in hydro-metereological parameters showed two distinct climate periods during the time interval analyzed: a drier period between 1987 and 1997: and a wetter period between 1997 and 2008. At Óbidos station, annual rainfall (AR) of 300 mm, total annual rainfall (TAR) of 1850 mm and annual discharge (AD) of 346 000 m^3/s between 1987 and 1997, and higher rates of AR and AD, 440 mm (TAR of 2200 mm) and 348 000 m^3/s, respectively, between 1997 and 2008 (Figure 7d), clearly define these two climate phases. At the Araguari, the AD also presented low rates with 1850 m^3/s between 1987 and 1997, and high rates with 2000 m^3/s between 1997 and 2008, as well as, at the Cassiporé River, with 310 m^3/s between 1987 and 1997, and 410 m^3/s between 1997 and 2008 (Figures 7d and 7e). At the Calçoene and Cunani coast, the drier time interval results in low rates of AR about 610 mm (TAR of 3440 mm) and 490 mm (TAR of 3250 mm), respectively. Conversely, the wetter period corresponded to AR of 790 mm (TAR of 4670 mm) and 670 mm (TAR of 3780 mm), respectively (Figure 7f).

Regarding the morphological and geobotanical units, the main changes in the Pleistocene plain occurred in 'várzea' and savannah areas with a complex network of meandering paleochannels. The 'várzea' covered an area of approximately 185 km^2 between 1987 and 1997, which had increased by 5·3 km^2 in 2008. Savannah areas showed a slight net increase of 1.6 km^2 between 1987 and 1997. This increase is likely related to the abandonment of small tidal channels along the Calçoene River (Figures 8a and 8b). However, savannah lost an area of 10·9 km^2 between 1997 and 2008 (Table V), concomitant to the development of lakes on existing paleochannels, previously occupied by savannah (Figures 8b–8d). The progressive growth of the town of Calçoene apparently did not influence this process, since 'várzea' expanded over savannah after 1997. Furthermore, the irregular and multiple

Table III. Summary of facies descriptions and sedimentary processes at the study site

Facies	Description	Process
Peat (Pt)	Very dark gray organic deposit with decomposed and intact vegetable fibers.	Deposition and accumulation of vegetable debris indicating autochthonous source and reducing condition.
Bioturbated mud (Mb)	Greenish gray mud with many roots, root marks and vegetable debris· Herbaceous roots and root marks can also be locally observed.	Intense mixture of fine sediments by bioturbation.
Laminated mud (Ml)	Very light gray and greenish gray mud with plane-parallel lamination.	Alternation of flocculated and non-flocculated laminae deposited from suspension, and variations in the organic colloid content. Lighter tones may correspond to the presence of kaulinite.
Lenticular bedding (Hl)	Gray and greenish gray mud with single and connected flat lenses of fine to very fine sand.	Low energy flows with mud deposition from suspension, but with periodic sand inflows through migration of isolated ripples.
Wavy bedding (Hw)	Greenish gray, wavy mud laminae in alternation with ripple-bedded fine sand layers.	Equal periods of mud and sand deposition from suspension and bedload transport, respectively.
Flaser bedding (Hf)	Light gray fine sand with dark gray, thin laminae of mud on bottomset.	Predominance of sand deposition from traction currents and mud during slack water periods.
Inclined mud (Mi)	Inclined laminae of dark gray mud bounded by thin films of organic matter.	Lateral accretion with predominance of mud deposition from suspension.
Inclined heterolithic (Hi)	Parallel inclined thin laminae of fine sand and gray mud with dip of ~15º. Granules can be locally observed.	Lateral accretion with sand and mud deposited during low energy flows of a small-scale point bar.
Massive mud (Mm)	Greenish gray mud and locally subangular quartz granules.	The massive nature indicates channel waters with high suspended load. Considering the gravel class occurrence, granules are left behind, while mud moved as suspension clouds.
Cross-laminated sand (Sc)	Olive gray, well sorted, fine to very fine sand with ripple cross-lamination.	Migration of small ripples during low energy flows.
Bioturbated sand (Sb)	Pale olive fine sand with reddish and yellowish mottles, many herbaceous roots in growth position.	Sediment homogenization and mottling by biological activity and diagenic process, respectively.
Planar sand (Sp)	Alternation of dark gray (heavy minerals) and brown (light minerals) fine to very fine sand with plane-parallel lamination or low-angle cross-lamination.	Deposition of sand by swash and backwash on gently sloping surface.

shapes of savannah areas, with meandering features are not consistent with human interventions (e.g. Soares-Filho *et al.*, 2006). In this sector, the tidal-fluvial channel shows high lateral migration, typical of low-gradient rivers with elevated suspension load (e.g. Leopold and Wolman, 1957). The maximum rates of erosion and lateral accretion are ~ 9 m/yr (Figure 8d).

Herbaceous fields predominate in the coastal plain, but were affected by a reduction in area of 2·6 km^2 between 1987 and 1997, and 1·8 km^2 between 1997 and 2008 (Table V). Flooded forests with 'várzea' and mangrove species (Vz/Mg) were relatively stable during 1987–1997 interval, but they presented a net loss area of about 3·8 km^2 between 1997 and 2008. Mangroves, however, expanded over the inundated field in the northern sectors of the Calçoene River, with migration rates near 21 m/yr (Figures 9a–9c). Additionally, mangrove expansion over mixed flats near the mouth of the Calçoene River occurred at rates of 10 to 100 m/yr between 1987 and 1997, increasing to 30 to 130 m/yr between 1997 and 2008 (Figure 9d). ETMB and tidal mud flats were also substrates for the development of mangroves between 1997 and 2008 (Figure 9d). However, mangrove erosion at a rate of approximately 30 m/yr between 1987 and 1997, decreasing to 5 m/yr between 1997 and 2008, can be observed in the northern sectors of the mouth of the Calçoene River (Figures 9d and 9e).

Chenier ridges are characterized by a generally erosive trend with a reduction in area of 0·6 km^2 between 1987 and 1997, and 0·2 km^2 between 1997 and 2008, mainly in the north of the study site (Figures 9b and 9e).

Discussion

Temporal changes in surface area

The expansion and accretion profiles may be related to the formation of secondary channels and muddy substrates suitable for colonization by pioneer species of mangrove, and the contraction and erosion profiles to abandonment and silting of tidal channels and tidal-fluvial channel migration, followed by the development of extensive cut banks. In the case of mangrove expansion near the mouth of the Calçoene River, the hydrodynamic perturbation of the mean alongshore coastal currents generated by river discharge and tidal outflow from some rivers along the Amazon-Guianas coast can result in the immobilization of parts of a migrating shoreface-attached mud bank, leading to the creation of extensive mudflats, since these mud banks and their associated fluid mud have a damping effect to incident wave energy (e.g. Jiang and Mehta, 1996; Plaziat and Augustinus, 2004). Thus, the arrival of a new mud bank may be associated with the formation of a mudflat several kilometers in area that is rapidly fringed by *Avicennia germinans* mangrove (Lefebvre *et al.*, 2004). This mangrove species can grow very rapidly (~2 m/yr; Anthony *et al.*, 2010), which amplifying the trapping effect of sediment, stabilizing the substrate to subsequent flood and increasing bed level elevation (e.g. Lefebvre *et al.*, 2004).

The chenier ridges displays ancient coastlines and the interruption of mud flat progradation (e.g. Augustinus, 1989; Silveira, 1998). Some of the existing chenier ridges were reworked by wave action and some ridges were isolated by

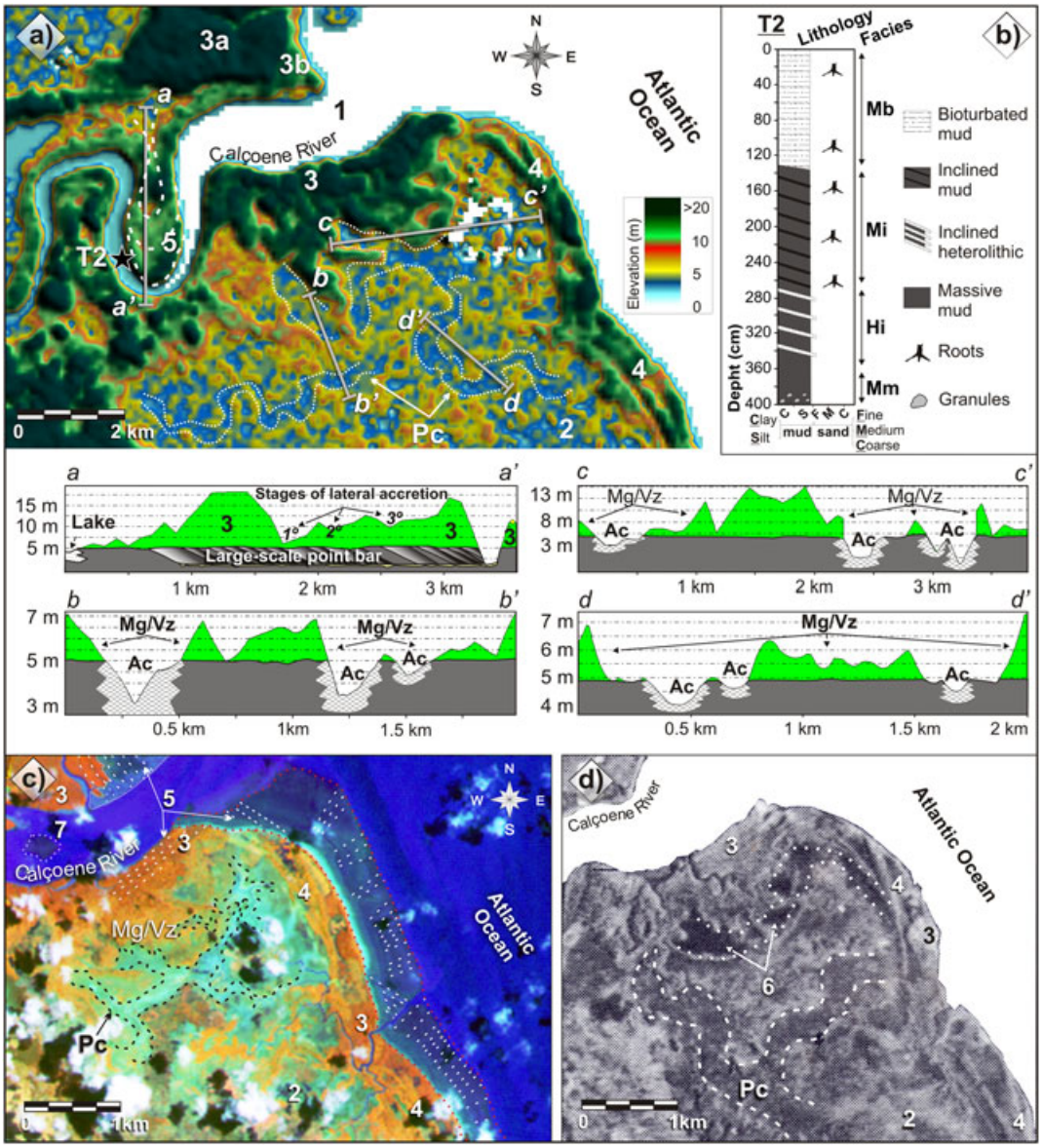

Figure 5. (a) Digital elevation model based on SRTM data showing tidal-fluvial channel with meandering – apparent "straight" segments and funnel-shaped morphology (1), and depositional environments of the coastal plain with morphometric profiles of large-scale point bar (a–a') and abandoned channels (Ac: b–b', c–c', d–d'); (b) Graphic sedimentary log of large-scale point bar – T2; (c) and (d) Landsat and GEMS 1000 images: inundated field (2), older and younger mangroves (3a and 3b of Figure 5a, respectively) chenier ridges (4), lateral and longitudinal accretion lines (5), lakes associated with abandoned channels (6) and elongated tidal mud bar (ETMB; 7). This figure is available in colour online at wileyonlinelibrary.com/journal/espl

mud flat accretion. Such processes were also observed in the Guiana, Suriname and the French Guiana coasts, where the northwestern migration of mud banks and inter-banks allowed the evolution of accretion and erosive profiles, respectively (Prost, 1989; Augustinus *et al.*, 1989).

Batista *et al.* (2009) quantified accretion and erosion along the Orange and Cassiporé cape in the Amapá coast from 1980 to 2003 and showed that the largest erosion rates had occurred next to the Cassiporé cape, with a mean retreat of 27·5 m/yr and erosion of 1·37 km^2/yr of mangrove area. However, the largest rates of sediment deposition had occurred in the Orange Cape, where the coast accreted 24·6 m/yr, adding 55·9 km^2 of mangrove area to shoreline. Gardel and Gratiot (2005) suggested that the mangrove forest of Kourou creek, French Guiana, which had a cross-shore width of 3 km in 1987, had totally disappeared by 2002 (~187·5 m/yr). The shoreline evolution trends of the Kaw study area, French Guiana, from 1981 to 1992 were marked by a retreat of 500 to 700 m induced by a reduction in the width of the spit-like zone (~45 m/yr to 63 m/yr). Between 1992 and 1999, a mud bank welded onto the eroded mudcape base, forming Kaw Point (Lefebvre *et al.*, 2004). These morphodynamic events also correlate with alternating mud-bank and inter-bank periods previously documented along this coast (Froidefond *et al.*, 1988).

The mud banks undergo migration over decadal time frames (Froidefond *et al.*, 1988), related to the supply of sediment from the Amazon River and wind pattern and intensity, which affects the wave regime on the coast of Amapá. The most rapid migration rates are observed in regions where the orientation of the trade winds tends to be alongshore. Thus, mud banks migrate faster in Surinam and in Guiana than in French Guiana (Augustinus, 1987; Eisma *et al.*, 1991). Additionally, the littoral is easily eroded when mud banks migrate (e.g. Allison *et al.*, 2000). However, significant phases of increased wave energy are accompanied by higher long-term (annual) rates of longshore mud bank migration, and the correlation is rather poor between the wave forcing parameter and migration rates

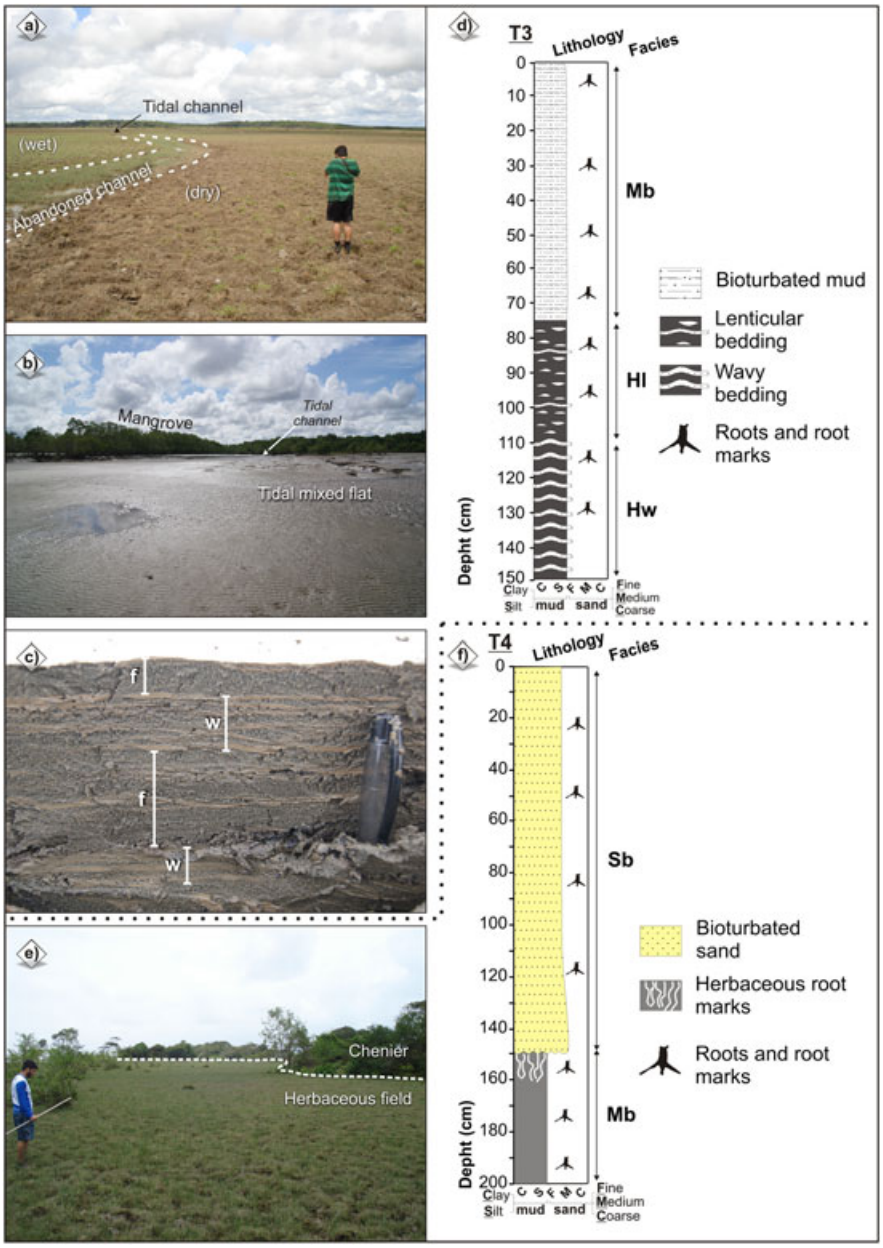

Figure 6. (a) Inundated field with dry and wet sectors due to the abandonment of a tidal channel; (b) surface relationship between mangrove, tidal mixed flat and tidal channel in advanced stages of silting; (c) detail of typical facies of tidal flats, f: flaser and w: wavy; (d) graphic sedimentary log of vegetated tidal flats – T3; (e) and (f) surface and vertical (T4) relationship of chenier and inundated field. This figure is available in colour online at wileyonlinelibrary.com/journal/espl

Table IV. The corresponding *t*-values and *p*-values for the two sample *t*-test for each group of seasonal (dry versus rainy) and temporal (drier versus wetter) patterns to each local station

	LMF		LMF		RDD		RDD	
	Seasonal		Temporal		Seasonal		Temporal	
Local station	*t*-Values	*p*-Values	*t*-Values	*p*-Values	*t*-Values	*p*-Values	*t*-Values	*p*-Values
Calçoene	5·1258	0·0002	–2·1951	0·9775	—	—	—	—
Cunani	–5·8396	0·9999	–1·2693	0·8882	—	—	—	—
Obidos	5·4643	0·9997	–0·0807	0·5318	–0·3329	0·6268	–0·0516	0·5203
Araguari	—	—	—	—	0·8863	0·8863	1·0127	0·1618
Cassiporé	—	—	—	—	–1·6238	0·9310	–4·0474	0·9993

because stronger wave forcing is generally associated with low angles of wave incidence. This suggests a complementary role for other hydrodynamic mechanisms in longshore mud bank migration (Gratiot *et al.*, 2007), such as changes in tidal amplitude and river discharge (e.g. Wells and Coleman, 1981; Gratiot *et al.*, 2008; Anthony *et al.*, 2010).

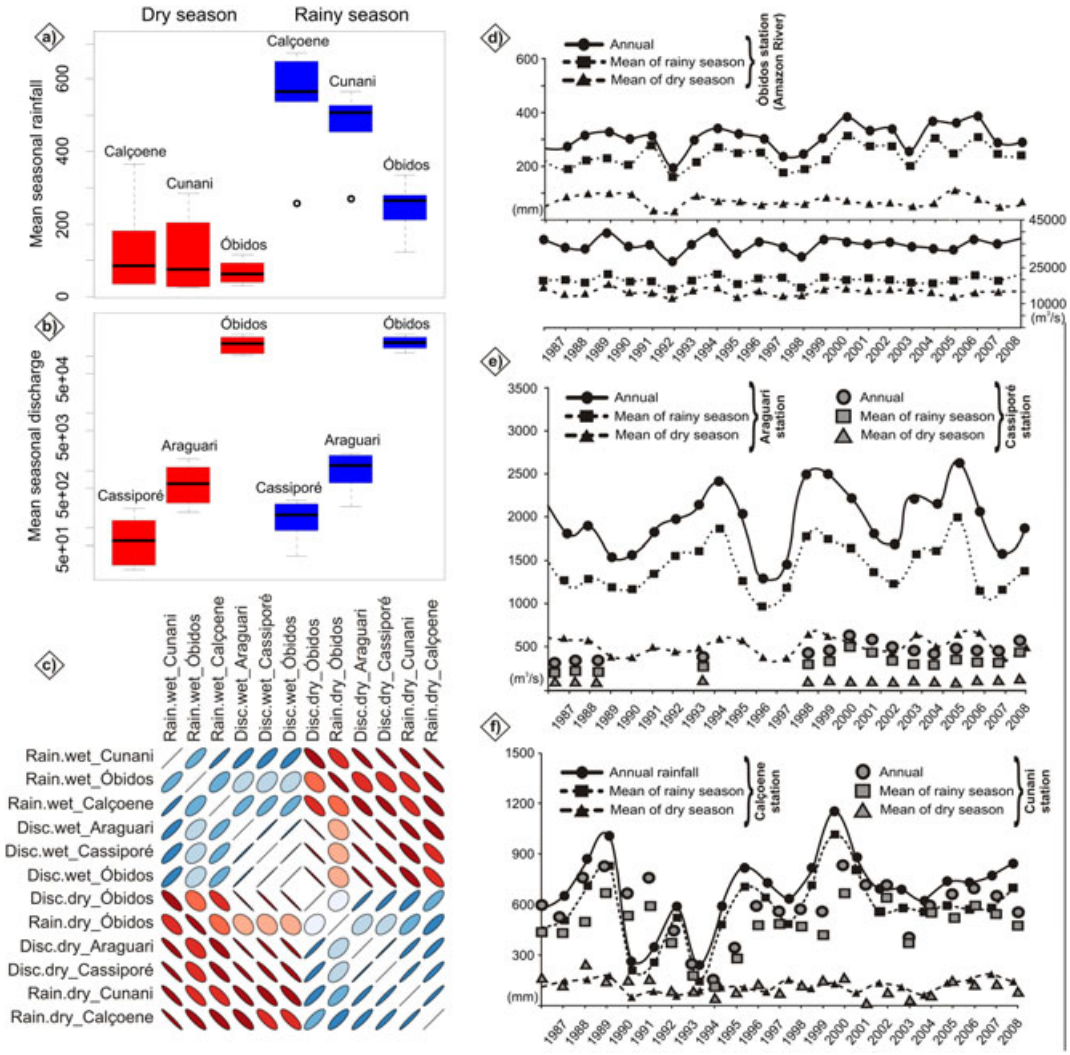

Figure 7. (a) Box plot showing mean seasonal rainfall from 1987 until 2008 at Calçoene and Cunani (Amapá coast), and Óbidos station (Amazon River); (b) box plot showing mean seasonal discharge in logaritimic scale from 1987 until 2008 at Cassiporé and Araguari (Amapá coast), and Óbidos station (Amazon River); (c) correlation plot of the hydrometeorological parameters used in this work, Rain: rainfall; Disc: discharge; wet: rainy season; dry: dry season; circles inclined to the right and circles inclined to the left represent positive and negative correlation, respectively; the correlation coefficient between the parameters will be greater when ellipses become progressively thinner (positive or negative); (d) annual, mean rainy and drier season rainfall and discharge at Óbidos sation – Amazon River; (e) annual, mean rainy and drier season discharge at the Araguari and Cassiporé stations; (f) annual, mean rainy and drier season rainfall at the Calçoene station. This figure is available in colour online at wileyonlinelibrary.com/journal/espl

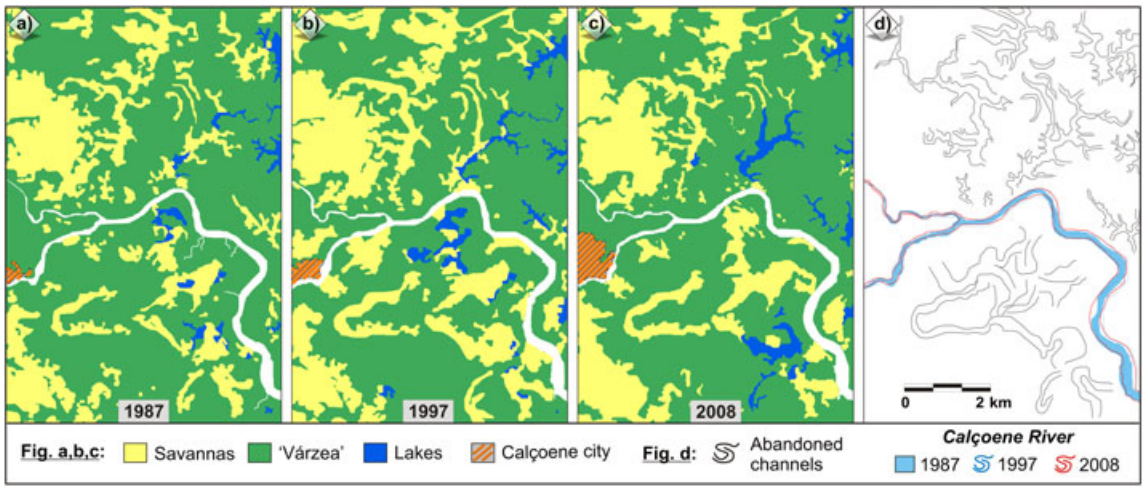

Figure 8. (a), (b) and (c) Changes in savannah, 'várzea' and lake areas and, (d) relationship with abandoned (secondary) channels of the coastal plain, beyond lateral migration of the tidal-fluvial channel between 1987, 1997, and 2008. This figure is available in colour online at wileyonlinelibrary.com/journal/espl

Table V. Changes in morphological and geobotanical units between 1987, 1997, and 2008

Geobotanical and morphological units	1987		1997		2008		Changes between 1987 to 1997		Changes between 1997 to 2008	
	km^2	%	km^2	%	km^2	%	km^2	%	km^2	%
'Várzea'	185·2	39	185·5	39	190·9	40	+0·3	+0·2	+5·3	+2·9
Savannah	112·5	24	114·1	24	103·2	21	+1·6	+1·4	–10·9	–9·6
Herbaceous field	71·8	15	69·2	15	67·4	14	–2·6	–3·6	–1·8	–2·6
Tidal mixed flat	31·2	6·6	35·7	7·5	37·1	7·7	+4·6	+14·4	+1·4	+3·9
Mangrove	31·3	6·6	32·0	6·7	36·7	7·6	+0·7	+2·2	+4·7	+14·7
Flooded forests with mangrove and 'várzea' species (Vz/Mg)	21·5	3·7	21·7	4·5	17·9	4·6	+0·2	+0·9	–3·8	–17·5
Chenier	10·9	2·3	10·7	2·2	10·1	2·1	–0·2	–1·8	–0·6	–5·6
Lakes	3·1	0·7	3·1	0·6	16·3	3·4	0·0	0·0	+13·2	+426
Tidal mud flat	0·1	0·0	1·9	0·4	0·7	0·1	+1·8	+1800	–1·2	–75

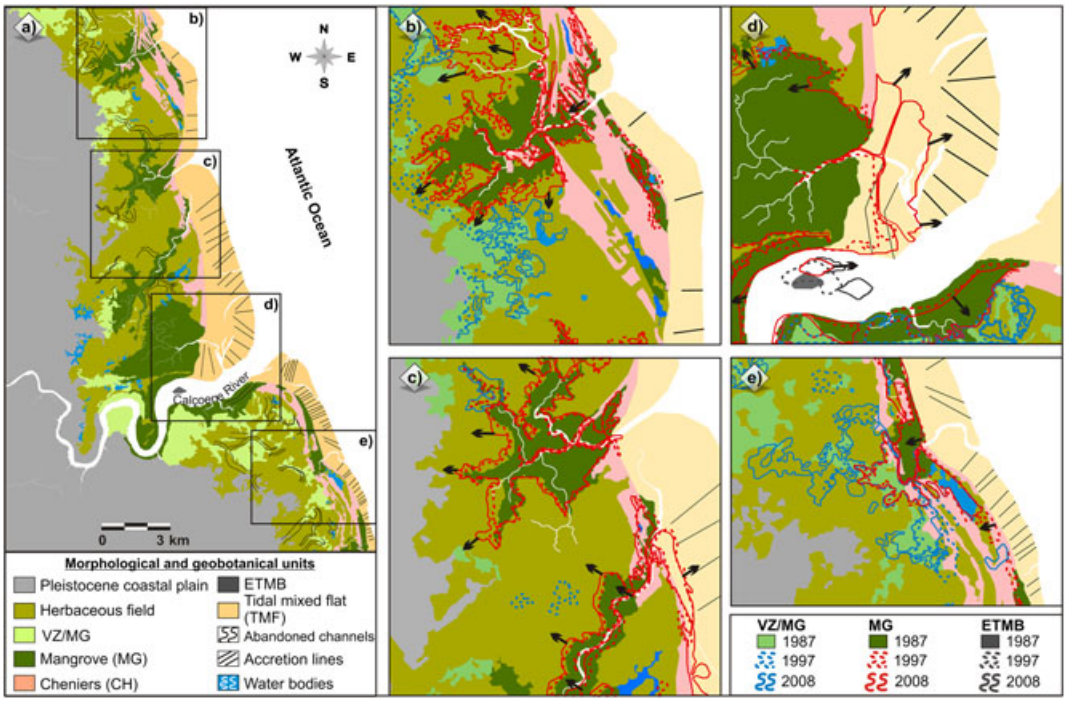

Figure 9. (a) Geomorphology of the Calçoene coastal plain in 1987, (b), (c), (d) and (e) changes in the morphological and geobotanical units between 1987, 1997, and 2008 with directional vector of the morphological and geobotanical migration with background images related to units in 1987, dashed lines to units in 1997 and solid lines to units in 2008. This figure is available in colour online at wileyonlinelibrary.com/journal/espl

Influence of climate and hydrological variability on the coastal setting

During the drier period, between 1987 and 1997, a shrinking in the area of the inundated field (–3·6%) took place in the study area. The area covered by freshwater wetlands was relatively stable, while 'várzea' and flooded forests with mangrove and 'várzea' species (Vz/Mg) changed by approximately +0·2% and +0·9%, respectively (Table V). The brackish water wetland represented by the mangrove underwent a relatively small expansion of 2·2%. This relatively dry period also resulted in the expansion of the savannah by approximately 1·4%. Subsequently, the wetter period between 1997 and 2008 likely contributed to the increase in size of the 'várzea' (+2·9%) and lakes (+426%) to the detriment of savannah (–9·5%), and mangrove expanded (+14·7%) over the inundated field (–2·6%) and tidal mud/mixed flats. Therefore, the decrease in rainfall index during the drier period (1987–1997) is well-correlated with the reduction of the Calçoene River discharge and jointly with increasing tidal amplitude related to the 18·5 yr nodal cycle favored the increase of migration rate of the mud bank and erosion profile along the littoral. It was followed by the increase of the Calçoene River discharge and jointly with decreasing tidal amplitude during the wetter period (1997–2008), which favored the development of mangroves on muddy substrates near the coastline as well as upstream.

The kilometer-scale mud bank and inter-bank profiles conform to those of accretion- or erosion-dominated muddy shore profiles (Kirby, 2000; Mehta, 2002). Inter-bank areas are identified by receding, low and concave erosion-dominated profiles of consolidated mud and sometimes chenier sands (e.g. Anthony *et al.*, 2010), while mud banks are recognized by prograding, high and convex accretion-dominated profiles of soft mud colonized by mangrove vegetation (Gratiot *et al.*, 2007). As demonstrated by Gardel and Gratiot (2005), mud-bank migration rates can vary both alongshore and in time (spatial-temporal), suggesting variations in the dynamic of mud-bank and inter-bank phases. Differences in migration rates are likely with interactions between climatic events and river discharge patterns (Anthony *et al.*, 2010; Gardel and Gratiot, 2005), such as for the Calçoene River.

Gratiot *et al*. (2008) estimate that the coastal sediment balance shows a deficit of about 37×10^6 tons/yr, resulting in shoreline retreat of about 30 m/yr over the period 1988–1999, and a reversion with excess of 35×10^6 tons/yr of shoreline sediment resulting in coastal progradation by about 200 m since 2000, which are well-correlated with the 18 · 5 yr nodal cycle.

The higher water levels may also allow higher incidence of wave-energy and erosion of the muddy coast and impact the capacity of mangroves to colonize topographically higher parts of the mud banks by diminishing bank-surface exposure to desiccation and leading to development of mud cracks that favor such colonization (Fiot and Gratiot, 2006; Proisy *et al*., 2009).

Changes in wetland distribution may reflect the coastal geomorphology (e.g. Fromard *et al*., 2004; Souza Filho *et al*., 2006; Lara and Cohen, 2009), since its development and expansion is determinate by the continent–ocean interaction, morphology, tidal regime, sea-level (Gornitz, 1991; Cohen and Lara, 2003; Guimarães *et al*., 2011) and the flow energy (Woodroffe *et al*., 1989). Therefore, coastal vegetation may be eroded and migrate landward due to higher inundation frequency. Similarly, internal vegetation domains on elevated mudflats will be subject to boundary adjustments, since mangroves would migrate to higher locations and could invade these areas, resulting in a stacking pattern of distal over proximal sedimentary facies (Cohen and Lara, 2003).

Conclusions

The integrated analysis allowed the identification of two distinct compartments on the Calçoene coast with morphological and geobotanical changes linked to the stabilization of savannah, 'várzea' and mangrove areas during the drier period with lower rainfall index between 1987 and 1997. The wetter period between 1997 and 2008 was characterized by a higher rainfall index that was associated with an increase in the area of 'várzea' and lakes over savannah, and the expansion of mangroves mainly over the inundated field and tidal mud/mixed flats. Therefore, the decrease in rainfall index during the drier period is well-correlated with the reduction of the Calçoene River discharge and jointly with increasing tidal amplitude related to the 18 · 5 yr nodal cycle, which favored an increase in the migration rates of the mud bank and erosion profile along the littoral. It was followed by an increase of the Calçoene River discharge and, jointly with decreasing tidal amplitude during the wetter period, this favored the development of mangroves on muddy substrates near the coastline as well as upstream. The changes of migration rates in time and space suggest alternations in the mud bank (accretion profiles) and inter-bank (erosion profiles) phases, and the differences in migration rates are likely associated with climatic changes, river discharge patterns and the 18 · 5 yr nodal cycle.

Acknowledgements—This work was funded by CNPq (Project 562398/2008-2). The first and second authors hold a scholarship from CNPq (Process 143518/2008-9 and 302943/2008-0). The authors thank members of the 'Laboratório de Dinâmica Costeira' and 'Grupo de Análises de Bacias Sedimentares da Amazônia' of the 'Universidade Federal do Pará', especially the sedimentologist MSc Luiz Saturnino de Andrade for numerous comments and suggestions that helped to significantly improve this manuscript. Thanks to Professor Dra Odete Fátima Silveira and Maria Thereza Prost for the aerial photographs used in this work.

References

Allen JRL. 1990. The Severn Estuary in southwest Britain: its retreat under marine transgression and fine sediment regime. *Sedimentary Geology* **66**: 13–28.

Allison MA, Lee MT. 2004. Sediment exchange between Amazon mudbanks and shore-fringing mangroves in French Guiana. *Marine Geology* **208**: 169–190.

Allison MA, Lee MT, Ogston AS, Aller RC. 2000. Origin of Amazon mudbanks along the northeastern coast of South America. *Marine Geology* **163**: 241–256.

Allison MA, Nittrouer CA, Kineke GC. 1995. Seasonal sediment storage on mudflats adjacent to the Amazon River. *Marine Geology* **125**: 303–328.

Amasseds. 1990. A multidisciplinary Amazon shelf sediment study. *EOS, Transactions of the American Geophysical Union* **71**: 1771–1777.

ANA. 2003. Agência Nacional de Águas. Sistema de Informações Hidrológicas. http://hidroweb.ana.gov.br/baixar/mapa/Bacia1.zip

ANA. 2010. Agência Nacional de Águas. Sistema de Informações Hidrológicas. http://hidroweb.ana.gov.br/Estacao.asp?Codigo=8250002

Anthony EJ, Dolique F. 2006. Intertidal subsidence and collapse features on wave-exposed, drift-aligned sandy beaches subject to Amazon mud: Cayenne, French Guiana. *Earth Surface Processes and Landforms* **31**: 1051–1057.

Anthony EJ, Gardel A, Gratiot N, Proisy C, Allison MA, Dolique F, Fromard F. 2010. The Amazon influenced muddy coast of South America: a review of mud-bank – shoreline interactions. *Earth-Science Reviews* **103**: 99–121.

Augustinus PGEF. 1987. The geomorphologic development of the coast of Guyana between the Corentyne River and the Esse-quibo River. In *International Geomorphology: Part. I*, Gardiner V (ed.). John Wiley & Sons: New York; 1281–1292.

Augustinus PGEF. 1989. Cheniers and chenier plains: a general introduction. *Marine Geology* **90**: 219–229.

Augustinus PGEF, Hazelhoff L, Kroon A. 1989. The chenier coast of Suriname: modern and geological development. *Marine Geology* **90**: 269–281.

Baltzer F, Allison M, Fromard F. 2004. Material exchange between the continental shelf and mangrove coasts with special reference to the Amazon-Guianas coast. *Marine Geology* **208**: 115–126.

Basan PB, Frey RW. 1978. Actual-paleontology and neoichnology of salt marches near Sapelo Island, Georgia. In *Trace fossils 2*, Crimes TP, Harper JC (eds). Seel House Press: Liverpool; 41–70 pp.

Batista EM, Souza Filho PWM, Silveira OFM. 2009. Avaliação de áreas deposicionais e erosivas em cabos lamosos da zona costeira Amazônica através da análise multitemporal de imagens de sensores remotos. *Revista Brasileira de Geofísica* **27**: 83–96.

Beardsley RC, Candela J, Limeburner R, Geyer WR, Lentz SJ, Castro BM, Cacchione D, Carneiro N. 1995. The M2 tide on the Amazon shelf. *Journal of Geophysical Research* **100**: 2283–2319.

Bezerra PEL, Oliveira W, Regis WDE, Brazão JEM, Gavinho J, Coutinho RCP. 1990. Amazônia legal: zoneamento das potencialidades e dos recursos naturais. In *Instituto Brasileiro de Geografia e Estatística, Superintendência de Desenvolvimento da Amazônia*. Projeto zoneamento das potencialidades dos recursos naturais da Amazônia: geologia, solos e vegetação. Div. 5: Rio de Janeiro; 9–89.

Câmara G, Souza RCM, Freitas UM, Garrido J. 1996. SPRING: integrating remote sensing and GIS by object-oriented data modeling. *Computers and Graphics* **20**: 395–403.

Carvalho FP, Costa Neto SV, Costa WJP, Coutinho RS, Figueira ZR, Figueiredo SL, Martins MHA, Santos VF, Silva AQ, Silva LMA, Silva MS, Silveira OFM, Takyiama LR. 2006. *Atlas Zoneamento Costeiro Estuarino do Estado do Amapá*. Macapá, PNMA/SQA/MMA; 77 pp.

Chappell JMA, Woodroffe CD. 1994. Macrotidal estuaries. In *Coastal Evolution: Late Quaternary Shoreline Morpho-dynamics*, Carter RWG, Woodroffe CD (eds). Cambridge University Press: Cambridge; 539 pp.

Chavez PS. 1988. An improved dark-object subtraction technique for atmospheric scattering correction of multispectral data. *Remote Sensing of Environment* **24**: 450–479.

Chavez PS, Berlin GL, Sowers LB. 1982. Statistical method for selecting Landsat MSS ratios. *Journal of Applied Photographic Engineering* **8**: 23–30.

Cohen MCL. 2003. *Past and Current Mangrove Dynamics on the Bragança Peninsula, Northern Brazil*, PhD Thesis, Center for Tropical Marine Ecology, University of Bremen; 110 pp.

Cohen MCL, Lara RJ. 2003. Temporal changes of vegetation boundaries in Amazonia: application of GIS and Remote sensing techniques. *Wetlands Ecology and Management* **11**: 223–231.

Cohen MCL, Souza Filho PWM, Lara RJ, Behling H, Angulo RJ. 2005. A model of Holocene mangrove development and relative sea-level changes on the Bragança Peninsula (northern Brazil). *Wetlands Ecology and Management* **13**: 433–443.

Cooley SR, Coles VJ, Subramaniam A, Yager PL. 2007. Seasonal variations in the Amazon plume-related atmospheric carbon sink. *Global Biogeochemical Cycles* **21**: GB3014.

Costa JB, Hasui Y, Bemerguy RL, Soares-Júnior AV, Villegas J. 2002. Tectonics and paleogeography of the Marajó Basin, northern Brazil. *Anais da Academia Brasileira de Ciências* **74**: 519–531.

Costa Neto SV, Silva MS. 2004. *Vegetação do setor costeiro estuarino do estado do Amapá. Instituto de Pesquisas Científicas e Tecnológicas do Estado do Amapá. Governo do Estado do Amapá. Cap. 5*. Projeto Zoneamento Econômico-Ecológico do setor costeiro estuarino: diagnóstico sócio ambiental participativo do setor costeiro estuarino; 72–96.

CPRM. 2010. Serviço Geológico do Brasil. Sistema de Informação Geológica. http://geobank.sa.cprm.gov.br/

Dalrymple RW, Knight RJ, Lambiase JJ. 1978. Bedforms and their hydraulic stability relationships in a tidal environment, Bay of Fundy, Canada. *Nature* **275**: 293–307.

Dalrymple RW, Knight RJ, Zaitlin BA, Middleton GV. 1990. Dynamics and facies model of a macrotidal sand-bar complex, Cobequid Bay – Salmon River estuary (Bay of Fundy). *Sedimentology* **37**: 577–612.

DHN. 2009. Diretoria de Hidrografia e Navegacão, Tábuas de Marés do ano de 2009. http://www.mar.mil.br/dhn/chm/tabuas/index.htm

DNPM. 1971. *Projeto RadamBrasil. Levantamento de recursos naturais*, v. 21, 23 e 24. Folhas: NA22, MACAPA. MME/DNPM: Rio de Janeiro.

Eisma D, Augustinus PGEF, Alexander CR. 1991. Recent and subrecent changes in the dispersal of Amazon mud. *Netherlands Journal of Sea Research* **28**: 181–192.

ESRI. 2006. *ArcGIS Version 9.0 Software*. ESRI: Redland, CA.

Fiot J, Gratiot N. 2006. Structural effects of tidal exposure on mud flats along the French Guiana coast. *Marine Geology* **228**: 25–37.

Froidefond JM, Pujos M, Andre X. 1988. Migration of mud-banks and changing coastline in French Guiana. *Marine Geology* **84**: 19–30.

Fromard F, Vega C, Proisy C. 2004. Half a century of dynamics coastal change affecting mangrove shorelines of French Guiana. A case study based on remote sensing analyses and field surveys. *Marine Geology* **208**: 265–280.

Gallo MN, Vinzon S. 2005. Generation of over tides and compound tides in Amazon estuary. *Ocean Dynamics* **55**: 441–448.

Gardel A, Gratiot N. 2005. A satellite image-based method for estimating rates of mud bank migration, French Guiana, South America. *Journal of Coastal Research* **21**: 720–728.

Global Mapper LLC. 2009. *Global Mapper Version 9.0 Software*. Global Mapper LLC: Parker, CO.

Gornitz V. 1991. Global coastal hazards from future sea level rise. *Palaeogeography, Palaeoclimatology, Palaeoecology* **89**: 379–720.

Gratiot N, Anthony EJ, Gardel A, Gaucherel C, Proisy C, Wells JT. 2008. Significant contribution of the 18.6 year tidal cycle to regional coastal changes. *Nature Geosciences* **1**: 169–172.

Gratiot N, Gardel A, Anthony EJ. 2007. Trade-wind waves and mud dynamics on the French Guiana coast, South America: input from ERA-40 wave data and field investigations. *Marine Geology* **236**: 15–26.

Guimarães JTF, Cohen MCL, França MC, Lara RJ, Behling H. 2010. Model of wetland development of the Amapá coast during the late Holocene. *Anais da Academia Brasileira de Ciências* **82**: 451–465.

Guimarães JTF, Cohen MCL, França MC, Pessenda LCR, Behling H. 2013. Morphological and vegetation changes on tidal flats of the Amazon Coast during the last 5000 cal yr BP. *The Holocene* **23**(4): 526–541. doi:10.1177/0959683612463097

Guimarães JTF, Cohen MCL, Pessenda LCR, França MC, Smith CB, Nogueira ACR. 2011. Mid and late Holocene sedimentary process and palaeovegetation changes near the mouth of the Amazon River. *The Holocene* **21**(8): 1–15.

Hayakawa EH, Rossetti DF, Valeriano MM. 2010. Applying DEM-SRTM for reconstructing a late Quaternary paleodrainage in Amazonia. *Earth and Planetary Science Letters* **297**: 262–270.

Hofton M, Dubayah R, Blair JB, Rabine D. 2006. Validation of SRTM elevations over vegetated and non-vegetared terrain using medium footprint Lidar. *Photogrammetric Engineering and Remote Sensing* **72**: 279–285.

IBGE. 2008. Mapa Geomorfológico do Estado do Amapá. Instituto Brasileiro de Geografia e Estatística – Coordenação de Pesquisas Naturais e Estudos Ambientais. ftp://geoftp.ibge.gov.br/mapas/tematicos/tematico_estadual/AP_geomorfologia.pdf

Jiang F, Mehta AJ. 1996. Mud banks of the southwest coast of India. V: Wave attenuation. *Journal of Coastal Research* **12**: 890–897.

Kirby R. 2000. Practical implications of tidal flat shape. *Continental Shelf Research* **20**: 1061–1077.

Kjerfve B, Lacerda LD. 1993. Mangroves of Brazil. In *Conservation and sustainable utilization of mangroves forests in Latin America and Africa regions. Part 1: Latin America*, ITTO/ISME Project PD114/90 (F). ITTO/ISME: Nishihara; 245–272.

Klein GV. 1970. Deposition and dispersal dynamics of intertidal sandbars. *Journal of Sedimentary Petrology* **40**: 1095–1127.

Klein GV. 1971. A sedimentary model for determining paleotidal range. *Geological Society of America Bulletin* **82**: 2585–2592.

Klein GV. 1977. *Clastic Tidal Facies*. Continuing Education Publication Company: Champaign, IL; 149 pp.

Lara RJ, Cohen MCL. 2009. Palaeolimnological studies and ancient maps confirm secular climate fluctuations in Amazonia. *Climatic Change* **94**: 399–408.

Lefebvre JP, Dolique F, Gratiot N. 2004. Geomorphic evolution of a coastal mudflat under oceanic influences: an example from the dynamic shoreline of French Guiana. *Marine Geology* **208**: 191–205.

Lentz SJ. 1995. The Amazon River plume during AMASSEDS: subtidal current variability and the importance of wind forcing. *Journal of Geophysical Research* **100**: 2377–2390.

Lentz SJ, Limeburner R. 1995. The Amazon River Plume during AMASSEDS: spatial characteristics and salinity variability. *Journal of Geophysical Research* **100**: 2355–2375.

Leopold LB, Wolman MG. 1957. *River Channel Patterns: Braided, Meandering and Straight. Physiographic and Hydraulic Studies of Rivers*, US Geological Survey Professional Paper 282B. US Geological Survey: Reston, VA; 39–85.

Lesourd S, Lesueur P, Brun-Cottan JC, Garnaud S, Poupinet N. 2003. Seasonal variations in the characteristics of superficial sediments in a macrotidal estuary (the Seine inlet, France). *Estuarine, Coastal and Shelf Science* **58**: 3–16.

Lessa GC, Masselink G. 1995. Sedimentation and hydrodynamic changes in a back-barrier macrotidal estuary: a morphodynamic approach. *Marine Geology* **129**: 25–45.

Lima MIC, Bezerra PE, Araújo HJT. 1991. Sistematização da Geologia do Estado do Amapá. In *Simpósio de geologia da Amazônia*, vol. 3, Anais, SBG: Belém; 322–335.

Martinez JM, Guyot JL, Filizola N, Sondag F. 2009. Increase in sediment discharge of the Amazon River assessed by monitoring network and satellite data. *Catena* **79**: 257–264.

McGregor GR, Nieuwolt S. 1998. *Tropical Climatology*, 2nd edition. John Wiley & Sons: New York; 339 pp.

Meade RH, Dunee T, Richey JE, Santos UM, Salati E. 1985. Storage and remobilization of suspended sediment in the lower Amazon River of Brazil. *Science* **228**: 488–490.

Mehta AJ. 2002. Mudshore dynamics and controls. In *Muddy Coasts of the World: Processes, Deposits and Function: Proceedings in Marine Science*, 4, Heal YT, Wang Y, Healy JA (eds). Elsevier: Amsterdam; 19–60.

Miall AD. 1978. Facies types and vertical profile models in braided river deposits: a summary. In *Fluvial Sedimentology*, Miall AD (ed.). Canadian Society of Petroleum Geologists: Calgary; 597–604.

Nittrouer CA, Kuehl SA. 1995. Geological significance of sediment transport and accumulation on the Amazon continental shelf-preface. *Marine Geology* **125**: 175–176.

Nittrouer CA, Kuehl SA, Sternberg RW, Figueiredo AG, Faria LEC. 1995. An introduction to the geological significance of sediment transport and accumulation on the Amazon continental shelf. *Marine Geology* **125**: 177–192.

Pianca C, Mazzini PLF, Siegle E. 2010. Brazilian offshore wave climate based on NWW3 reanalysis. *Brazilian Journal of Oceanography* **58**: 53–70.

Plaziat J-C, Augustinus PGEF. 2004. Evolution of progradation/erosion along the French Guiana mangrove coast: a comparison of mapped shorelines since the 18th century with Holocene data. *Marine Geology* **208**: 127–143.

Prost MT. 1989. Coastal dynamics and chenier sands in French Guiana. *Marine Geology* **90**: 259–267.

Proisy C, Gratiot N, Anthony EJ, Garde LA, Fromard F, Heuret P. 2009. Mud bank colonization by opportunistic mangroves: a case study from French Guiana using lidar data. *Continental Shelf Research* **29**: 632–641

Pugh DT. 1987. *Tides, Surges and Mean Sea-level: A Handbook for Engineers and Scientists*. John Wiley & Sons: London; 486 pp.

Reineck HE. 1975. German North Sea tidal flats. In *Tidal Deposits: A Casebook of Recent Examples and Fossil Counterparts*, Ginsburg RN (ed.). Springer-Verlag: New York; 5–12.

Reineck HE, Singh IB. 1980. *Depositional Sedimentary Environments with Reference to Terrigenous Clastics*, 2nd edition. Springer-Verlag: Berlin; 542 pp.

Rosario RP, Bezerra MOM, Vinzon SB. 2009. Dynamics of the saline front in the Northern Channel of the Amazon River – influence of fluvial flow and tidal range (Brazil). *Journal of Coastal Research* **2**: 503–514.

Santos VF. 2006. *Ambientes Costeiros Amazônicos: avaliação de Modificações por Sensoriamento Remoto*. Curso de Pós-Graduação em Geologia e Geofísica Marinha, Universidade Federal Fluminense: Tese de doutorado; 306 pp.

Silveira OFM. 1998. *A Planície costeira do Amapá: dinâmica de ambiente costeiro influenciado por grandes fontes fluviais quaternárias*. Programa de Pós-Graduação em Geologia e Geoquímica, Universidade Federal do Pará: Tese (Doutorado em Geologia); 215 pp.

Soares-Filho BS, Nepstad D, Curran L, Voll E, Cerqueira G, Garcia RA, Ramos CA, Mcdonald A, Lefebvre P, Schlesinger P. 2006. Modeling conservation in the Amazon basin. *Nature* **440**: 520–523.

Sommerfield CK, Nittrouer CA, Figueredo AG. 1995. Stratigraphic evidence of changes in Amazon shelf sedimentation during the late Holocene. *Marine Geology* **125**: 351–371.

Souza EJ. 2010. *Geologia da região costeira do Amapá com ênfase na estratigrafia, morfotectônica e geomorfologia*. Faculdade de Geologia, Universidade Federal do Pará. Monografia de Conclusão de Curso: Belém; 118 pp.

Souza Filho PWM, Cohen MCL, Lara RJ, Lessa GC, Koch B, Behling H. 2006. Holocene coastal evolution and facies model of the Bragança macrotidal flat on the Amazon Mangrove Coast, northern Brazil. *Journal of Coastal Research, Special Issue* **39**: 306–310.

Szatmari P, Françolin JBL, Zanotto O, Wolff S. 1987. Evolução tectônica da margem equatorial brasileira. *Revista Brasileira de Geociências* **17**: 180–188.

Thompson RW. 1975. Tidal flat sediments of the Colorado delta, northwestern Gulf of California. In *Tidal Deposits: A Casebook of Recent Examples and Fossil Counterparts*, Ginsburg RN (ed.). Springer-Verlag: New York; 57–65.

Van Straaten LMJU. 1961. Sedimentation in tidal flat areas. *Journal of the Alberta Society of Petroleum Geologists* **9**: 203–226.

Walker RG. 1992. Facies, facies models and modern stratigrahic concepts. In *Facies Models – Response to Sea Level Change*, Walker RG, James NP (eds). Geological Association of Canada: Ontario; 1–14.

Weimer RJ, Howard JD, Lindasay DR. 1982. Tidal flats and associated tidal channels. In *Sandstone Depositional Environments*, Scholle PA, Spearing D (eds). The American Association of Petroleum Geologists: Menasha, WI; 191–245.

Wells JT, Coleman JM. 1978. Longshore transport of mud by waves: northeastern coast of South America. *Netherlands Journal of Geosciences* **57**: 353–359.

Wells JT, Coleman JM. 1981. Periodic mudflat progradation, northeastern coast of South America: a hypothesis. *Journal of Sedimentary Petrology* **51**: 1053–1068.

Woodroffe CD, Chappell JMA, Thom BG, Wolanski E. 1989. Depositional model of a macrotidal estuary and floodplain, South Alligator River, northern Australia. *Sedimentology* **36**: 737–756.